

**DEVELOPMENT OF HIGH-RESOLUTION  
IMAGING METHODS FOR MYOSIN MOTOR  
STUDY**

**SNEHA KUMARI**



**DEPARTMENT OF BIOCHEMICAL ENGINEERING AND  
BIOTECHNOLOGY  
INDIAN INSTITUTE OF TECHNOLOGY DELHI  
AUGUST 2024**

© Indian Institute of Technology Delhi (IITD), New Delhi, 2024

**DEVELOPMENT OF HIGH-RESOLUTION  
IMAGING METHODS FOR MYOSIN MOTOR  
STUDY**

by

**SNEHA KUMARI**

DEPARTMENT OF BIOCHEMICAL ENGINEERING AND  
BIOTECHNOLOGY

Submitted

In fulfilment of the requirements of the degree of Doctor of Philosophy  
to the



**INDIAN INSTITUTE OF TECHNOLOGY DELHI**

**AUGUST 2024**

*Dedicated to My Parents*

## CERTIFICATE

This is to certify that the thesis titled “**Development of High-Resolution Imaging Methods for Myosin Motor Study,**” being submitted by **Ms. Sneha Kumari** to the Indian Institute of Technology Delhi for the award of the degree of **Doctor of Philosophy**, represents an original and authenticated work under my supervision and guidance performed by her under my supervision and guidance in compliance with the rules and regulations of Indian Institute of Technology Delhi.

To the best of my knowledge, the results embedded in this thesis have not been submitted and will not be submitted in part or full to this institute or any other institute or university for the award of any other degree or diploma.

Date

Dr. RaviKrishnan Elangovan  
Associate Professor  
Department of Biochemical  
Engineering and Biotechnology  
Indian Institute of Technology  
Delhi  
New Delhi - 110016

## ACKNOWLEDGMENTS

The entirety of my road toward a Ph.D. has been comprised of a predetermined assortment of complex and perceptible occurrences that have played a significant part in reshaping and transforming my identity. It was an incredible learning experience and would not have been accomplished without the invaluable support and encouragement of numerous people whom I would like to express my gratitude and honor.

To begin, I would like to express my profound gratitude to the Almighty GOD for all the blessings that have been a source of strength, inspiration, and solace during moments of challenge and triumph.

Next, I want to extend my deep respect and admiration to Prof. Ravi Krishnan Elangovan for his exceptional academic supervision and unwavering moral encouragement. I am eternally grateful for his insight, experience, and patience, which significantly influenced the direction of this research. I sincerely appreciate his fervor for science and diligent disposition, which has inspired and been a significant impetus for me during my Ph.D. studies. I would like to extend my sincere gratitude to him for generously dedicating his precious time and providing me with invaluable guidance. His consistent mentorship and modern critique have allowed me to develop and advance professionally and personally. I aspire to perpetuate his fervor in my future pursuits.

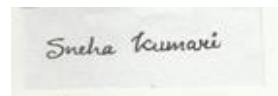
I want to thank my research committee members, Prof. Saroj Mishra, Prof. Preeti Srivastava, and Prof. Vivekanandan Perumal, for assessing my work and providing their invaluable recommendations for its enhancement. I express my gratitude to Dr. Amit Das, Dr. Saroj Kumar, and Prof. Kedar Khare for their collaboration and assistance in various aspects of this research project. I want to express my gratitude to Prof. Ritu Kulshreshtha, the Head of the Department, and the other faculty members of DBEB for their engaging instruction and unwavering assistance throughout the past five years.

I want to express my sincere gratitude to the Molecular Imaging and Diagnostics Lab personnel for their invaluable assistance and unwavering support over the past five years. I want to express my gratitude to Dr. Vidhu Soman Pillai and Jagat Narayan Prajapati, who provided valuable recommendations and support in overseeing the laboratory environment during the execution of this project. I am forever grateful for the assistance and companionship provided by my friends –

Ms. Arti Tyagi, Mrs. Neha Khaware, Ms. Ada Zwetlana, Ms. Shefali Singh, and Ms. Neelam Upadhyay - who fostered a conducive work atmosphere and offered unwavering support throughout my academic journey at IIT-Delhi. I have also been fortunate enough to have amazing friends Ms. Aakanksha Ahlawat, Ms. Rupsa Chatterjee, Ms. Priyanka Dubey, and Mr. Imran Ahmad for intellectual companionship and joyous moments. Gratitude is also owed to Ms. Ratnabali, Mr. Aayush, Ms. Rukmini, Mr. Jaykumar, and other laboratory members for their efforts in sustaining a vibrant atmosphere within the lab. I want to thank Mr. Prabhu Balasubramanian, Mr. Gaurav Jhakda, Mr. Ashutosh Pathak, Mr. Ramesh, and Ms. Himanshi Singh for their diligent management of the laboratory's needs and valuable support in handling financial transactions.

I thank the DBEB and KSBS laboratory personnel for permitting me to utilize specific instruments and for providing me with the valuable opportunity to improve my practical skills. I thank Mr. Suraj Mishra at Sonipat-IIT Delhi campus for his supervision in learning essential microscopy instrument support. I want to thank the Indian Institute of Technology Delhi and specifically the Department of Biochemical Engineering and Biotechnology for selecting me to join the IITD community and supporting me in doing this research. I am grateful to the Ministry of Human Resource and Development, Government of India, for financially supporting my five-year PhD studies.

Finally, I am grateful and fortunate to have the indispensable support system of my affectionate family, throughout the journey: my mother Mrs. Niloo Srivastava, my father Mr. Sadanand Srivastava, my highly encouraging siblings, Ms. Pallavi Kumari, Ms. Smrity Kumari and my supportive husband Mr. Aniket Srivastava. The everlasting love, encouragement, and support that my family has provided me with during this journey is something for which I am indebted to them. Their unwavering affection, concern, and backing have been a constant source of inspiration in my relentless quest for excellence. I attribute my accomplishments solely to the graces bestowed upon me by others, and I wholeheartedly devote this thesis to them.



Date:

Sneha Kumari

## ABSTRACT

This abstract describes developing a high-speed tracking method by modification in motor components for nanoparticle attachment. Myosin motors are nano-sized protein machines that power the movement that defines life. These miniature molecular devices serve as engines utilizing chemical energy stored in ATP to produce useful mechanical work in the form of a few nanometre displacement events leading to force generation that is required for cargo transport, cell division, and cell locomotion, translated to macroscopic movements like running, etc. The myosin superfamily is vast and varied, with complex and extensive groups of myosin proteins that are categorized into various classes based on their biological roles inside the cell. The present work is focussed on conventional myosin II, which has a low duty ratio and works in co-operativity.

With the advent of *in vitro* motility assay (IVMA), detailed functional studies of the actomyosin system could be performed. The major challenge with the currently available IVMA for tracking actin filaments is a resolution limitation of  $\pm 50\text{nm}$ . To overcome this, we have developed a single molecule IVMA in which nanoparticles (quantum dot) will be attached along actin filaments and visualized by a super-resolution microscopy system.

This thesis examines the kinetics of rhodamine phalloidin actin as a control data set, followed by the modification of actin by the use of biotin labeling, and finally, the attachment of nanoscale quantum dots to actin in order to investigate the mechanical properties of individual myosin II motors. The control data indicates that the speed at which actin slides increases as the density of myosin on the surface increases and is minimally affected by changes in temperature. The comparative velocity analysis was also performed with the biotin-labeled actin and non-biotin conjugated rhodamine phalloidin actin filament. Both the control and biotin-conjugated F actin gave similar sliding velocities and performed well in the *in vitro* motility assay. It was also discovered that the actin gliding velocity increased as the ATP concentration was raised.

The attachment of nanoscale cargo is based on biotin-streptavidin conjugation chemistry, i.e., biotin-conjugated actin filament was tagged with a streptavidin-coated quantum dot by precise optimization of monomer ratio during polymerization to achieve a single moving quantum dot in the *in vitro* motility assay for study. Using super-resolution microscopy, individual moving quantum dots (Qdots) were seen over time. The dual-channel visualization by Structured Illumination Microscopy, a super-resolution technique, utilizes sinusoidal light patterns to

illuminate the specimen and capture sample information at higher frequencies, resulting in a twofold improvement over the diffraction limit as compared to conventional microscopy systems. Quantum dots were then precisely located using an efficient algorithm with nm tracking accuracy in the 1.5 nm range. The Qdots were tracked as they moved along a surface covered with a skeletal myosin ii motor. The average velocity of Qdot-actin corresponds to the results obtained using actin labeled with rhodamine-phalloidin. So, conjugation was found to have an insignificant effect on motility.

This modified Qdot assay system allows a single-molecule study of the myosin motor and is, therefore, suitable for quantitatively estimating the individual step size of the motor during the assay. We have determined the myosin cross-bridges step size by measuring the quantum dots' slowly moving velocity at lower ATP concentration and low myosin surface density. So, this technology is well equipped to perform tracking with high precision in temporal resolution with significantly improved SNR (signal to noise ratio) compared to conventional set-up. Also, the nanoparticles (QD) attached to actin filament act as a point source of light offering ease in filament tracking compared to conventional manual tracking. Moreover, the cargo (QD) attachment to the thin filament allows for their precise transportation to designated locations on the chip, hence allowing a wide range of nano-technological applications.

**Keywords-** Actin, biotin actin, cargo, IVMA, Myosin motors, and Single-molecule system.

## सारांश

यह सार नैनोकण अनुलग्नक के लिए मोटर घटकों में संशोधन करके एक उच्च गति ट्रेकिंग विधि विकसित करने का वर्णन करता है। मायोसिन मोटर्स नैनो-आकार की प्रोटीन मशीनें हैं जो जीवन को परिभाषित करने वाली गति को शक्ति प्रदान करती हैं। ये लघु आणविक उपकरण कुछ नैनोमीटर विस्थापन घटनाओं के रूप में उपयोगी यांत्रिक कार्य का उत्पादन करने के लिए एटीपी में संग्रहीत रासायनिक ऊर्जा का उपयोग करने वाले इंजन के रूप में काम करते हैं, जिससे कार्गो परिवहन, कोशिका विभाजन और कोशिका गति के लिए आवश्यक बल उत्पन्न होता है, जिसे मैक्रोस्कोपिक आंदोलनों में अनुवादित किया जाता है। दौड़ना, आदि। मायोसिन सुपरफैमिली विशाल और विविध है, जिसमें मायोसिन प्रोटीन के जटिल और व्यापक समूह हैं जिन्हें कोशिका के अंदर उनकी जैविक भूमिकाओं के आधार पर विभिन्न वर्गों में वर्गीकृत किया गया है। वर्तमान कार्य पारंपरिक मायोसिन II पर केंद्रित है, जिसका कर्तव्य अनुपात कम है और सहकारीता में काम करता है।

इन विट्रो गतिशीलता परख (आईवीएमए) के आगमन के साथ, एक्टोमीओसिन प्रणाली का विस्तृत कार्यात्मक अध्ययन किया जा सकता है। एक्टिन फिलामेंट्स को ट्रेक करने के लिए वर्तमान में उपलब्ध IVMA के साथ प्रमुख चुनौती  $\pm 50\text{nm}$  की रिज़ॉल्यूशन सीमा है। इस पर काबू पाने के लिए, हमने एक एकल अणु आईवीएमए विकसित किया है जिसमें नैनोकणों (क्यूडी) को एक्टिन फिलामेंट्स के साथ जोड़ा जाएगा और एक सुपर-रिज़ॉल्यूशन माइक्रोस्कोपी प्रणाली द्वारा देखा जाएगा।

यह थीसिस एक नियंत्रण डेटा सेट के रूप में रोडामाइन फैलोलाइडिन एक्टिन के कैनेटीक्स की जांच करती है, इसके बाद बायोटिन लेबलिंग के उपयोग से एक्टिन में संशोधन होता है, और अंत में, व्यक्तिगत मायोसिन II के यांत्रिक गुणों की जांच करने के लिए एक्टिन में नैनोस्केल क्वांटम डॉट्स का जुड़ाव होता है। मोटर्स, नियंत्रण डेटा इंगित करता है कि सतह पर मायोसिन का घनत्व बढ़ने पर एक्टिन के फिसलने की गति बढ़ जाती है और तापमान में परिवर्तन से यह न्यूनतम रूप से प्रभावित होता है। तुलनात्मक वेग विश्लेषण बायोटिन-लेबल एक्टिन और गैर-बायोटिन संयुग्मित रोडामाइन फालोइडिन एक्टिन फिलामेंट के साथ भी किया गया था। नियंत्रण और बायोटिन-संयुग्मित एफ एक्टिन दोनों ने समान स्लाइडिंग वेग दिए और इन विट्रो गतिशीलता परख में अच्छा प्रदर्शन किया। यह भी पता चला कि एटीपी सांद्रता बढ़ने पर एक्टिन ग्लाइडिंग वेग बढ़ गया।

नैनोस्केल कार्गो का जुड़ाव बायोटिन-स्ट्रेप्टाविडिन संयुग्मन रसायन विज्ञान पर आधारित है, अर्थात्, इन विट्रो गतिशीलता में एकल चलती क्वांटम डॉट को प्राप्त करने के लिए पोलीमराइजेशन के दौरान मोनोमर अनुपात के सटीक अनुकूलन द्वारा बायोटिन-संयुग्मित एक्टिन फिलामेंट को स्ट्रेप्टाविडिन-लेपित क्वांटम डॉट के साथ टैग किया गया था। अध्ययन के लिए परख, सुपर-रिज़ॉल्यूशन माइक्रोस्कोपी का उपयोग करके, समय के साथ व्यक्तिगत गतिशील क्वांटम डॉट्स (क्यूडॉट्स) देखे गए। स्ट्रक्चर्ड इल्यूमिनेशन माइक्रोस्कोपी द्वारा दोहरे चैनल विजुअलाइजेशन, एक सुपर-रिज़ॉल्यूशन तकनीक, नमूने को रोशन करने और उच्च आवृत्तियों पर नमूना जानकारी कैप्चर करने के लिए साइंसॉइडल प्रकाश पैटर्न का उपयोग करती है, जिसके परिणामस्वरूप पारंपरिक माइक्रोस्कोपी सिस्टम की तुलना में विवर्तन सीमा में दोगुना सुधार होता है। क्वांटम डॉट्स को 1-2 एनएम रेंज में एनएम ट्रेकिंग सटीकता के साथ एक कुशल एल्गोरिदम का उपयोग करके सटीक रूप से स्थित किया गया था। Qdots को तब ट्रेक किया गया जब वे एक कंकाल मायोसिन II मोटर से ढकी सतह पर आगे बढ़ रहे थे। क्यूडॉट-एक्टिन का औसत वेग रोडामाइन-फैलोइडिन के साथ लेबल किए गए एक्टिन का उपयोग करके प्राप्त परिणामों से

मेल खाता है। इसलिए, संयुग्मन का मोती पर नगण्य प्रभाव पाया गया।

यह संशोधित Qdot परख प्रणाली मायोसिन मोटर के एकल-अणु अध्ययन की अनुमति देती है और इसलिए, परख के दौरान मोटर के व्यक्तिगत चरण आकार का मात्रात्मक अनुमान लगाने के लिए उपयुक्त है। हमने कम एटीपी सांद्रता और कम मायोसिन सतह घनत्व पर क्वांटम डॉट्स के धीरे-धीरे चलने वाले वेग को मापकर मायोसिन क्रॉस-ब्रिज चरण आकार निर्धारित किया है। इसलिए, यह तकनीक पारंपरिक सेट-अप की तुलना में काफी बेहतर एसएनआर के साथ अस्थायी रिज़ॉल्यूशन में उच्च परिशुद्धता के साथ ट्रेकिंग करने के लिए अच्छी तरह से सुसज्जित है। इसके अलावा, एक्टिन फिलामेंट से जुड़े नैनोकण (क्यूडी) पारंपरिक मैनुअल ट्रेकिंग की तुलना में फिलामेंट ट्रेकिंग में प्रकाश के एक बिंदु स्रोत के रूप में कार्य करते हैं। इसके अलावा, पतले फिलामेंट से कार्गो (क्यूडी) का जुड़ाव चिप पर विशिष्ट स्थानों पर उनके स्थानांतरण को सक्षम बनाता है, जिससे कई नैनो-तकनीकी अनुप्रयोगों की सुविधा मिलती है।

कीवर्ड- एक्टिन, बायोटिन एक्टिन, कार्गो, आईवीएमए, मायोसिन मोटर्स और एकल-अणु प्रणाली।

# CONTENT

CERTIFICATE.....	i
ACKNOWLEDGEMENTS .....	ii
ABSTRACT.....	iv
सारांश .....	vi
CONTENT.....	viii
LIST OF FIGURES .....	xiii
LIST OF TABLES .....	xxiii
ABBREVIATION AND SYMBOLS .....	xxiv
Chapter 1: Introduction .....	1
Objectives .....	6
Chapter 2: Theory and Background.....	8
2.1    Skeletal muscle architecture .....	9
2.1.1    Muscle fibers and myofibril .....	10
2.1.2    Sarcomere organization .....	11
2.1.3    Myosin thick filament structure and function.....	14
2.1.3    Actin thin filament structure and function.....	16
2.2    Mechanism of muscle contraction .....	21
2.3    Chemomechanical cycle.....	23
2.4    Kinetics of single actomyosin event .....	24
2.5    Fundamental properties of myosin ii motor .....	26
2.5.1    Duty ratio.....	26
2.5.2    Processivity.....	27

2.6	Bioengineering with actin protein .....	28
2.6.1	Actin labeling by non-covalent approach.....	28
2.6.2	Labelling by natural actin-binding proteins .....	29
2.6.3	Actin labeling by covalent approach .....	30
2.7	Fluorescence microscopy .....	31
2.8	Super-resolution microscopy .....	34
2.9	Significance of probe Reporter in single particle study .....	36
2.10	Particle localization and signal-to-noise ratio .....	38
2.11	Single-molecule power stroke studies .....	40
2.11.1	Single-step estimation using interference technique.....	41
2.11.2	Step size measurement using laser trap assay .....	42
2.11.3	Individual myosin manipulation and estimation of step size .....	43
2.11.4	A two-step power stroke estimation using high-speed AFM.....	43
2.11.5	Step-wise motor displacement by myosin in co-operation.....	45
2.11.6	Myosin <i>in vitro</i> step size tracked by super-resolution .....	45
2.12	Application and significance of molecular motor .....	47
Chapter 3 Materials and Methods .....		48
3.1	Materials .....	49
3.2	CONTROL IVMA ASSAY .....	50
3.2.1	Protein preparation .....	50
3.2.1.1	Myosin ii protein extraction .....	50
3.2.1.1	Actin protein extraction .....	51
3.2.1.1	Preparation of acetone powder .....	51
3.2.1.2	Isolation of actin protein .....	51
3.2.2	G actin polymerization and labeling .....	52
3.2.3	Analysis of purity and protein quantification .....	52
3.2.4	<i>In vitro</i> motility assay .....	52
3.2.4.1	Construction of flow cell .....	53
3.2.4.2	Gliding motility assay .....	53

3.2.5	Immobilized myosin surface density estimation .....	53
3.2.6	Image acquisition and microscopy .....	53
3.2.6.1	Imaging set up tool .....	54
3.2.6.2	Acquisition tool .....	54
3.2.6.3	Incubation tool .....	55
3.2.7	Moving Filament Data Analysis .....	55
3.2.8	Moving Filament Length Analysis .....	57
3.3	PROTEIN MODIFICATION AND LABELLING .....	57
3.3.1	Actin modification by biotin conjugation .....	58
3.3.1.1	Biotin conjugation .....	58
3.3.1.2	Buffer exchange using ultracentrifugation .....	58
3.3.1.3	F actin conjugation by EZ link sulfo NHS LC biotin .....	58
3.3.1.4	Removal of excess sulfo NHS LC biotin by buffer exchange .....	59
3.3.1.5	Calculation of moles of biotin per mole protein .....	59
3.3.2	F-actin labelling by alexa 488 dye .....	60
3.3.3	Removal of dead head in flow cell .....	60
3.3.4	Gliding motility assay with biotin conjugated actin .....	60
3.3.5	Image acquisition and microscopy .....	60
3.4	MODIFIED IVMA QDOT ASSAY .....	61
3.4.1	Optical charecterization of quantum dot .....	61
3.4.2	Modified IVMA Qdot assay .....	61
3.4.2.1	Preparation of myosin in soluble form .....	61
3.4.2.2	Single molecule QD motility assay .....	61
3.4.3	Super resolution image acquisition .....	62
3.4.3.1	Imaging set up tool .....	62
3.4.3.2	Acquisition tool .....	63

3.4.3.3	Dual channel imaging tool .....	63
3.4.4	QD data analysis .....	64
Chapter 4: Results and Discussion.....		67
4.1	CONTROL <i>IVMA</i> ASSAY RESULT .....	68
4.1.1	Purification analysis and quantification of protein .....	68
4.1.2	<i>In Vitro</i> motility assay with purified protein .....	69
4.1.2.1	Actin filament dynamics in <i>IVMA</i> .....	70
4.1.3	Effect of temperature on actin sliding velocity at varying myosin density .....	71
4.1.4	Effect of temperature on actin filament length at varying myosin density .....	73
4.1.5	Surface density estimation of myosin using SDS PAGE analysis .....	77
4.1.6	Effect of ATP concentration on actin filament sliding velocity at 30° C.....	78
4.1.8	Effect of ATP concentration on actin filament length .....	80
4.2	BIOTIN CONJUGATED ACTIN <i>IVMA</i> ASSAY RESULT .....	81
4.2.1	Purification analysis of biotin modified protein .....	82
4.2.2	Quantification by HABA assay and motility check .....	83
4.2.3	Effect of temperature on modified actin sliding velocity .....	84
4.2.4	Effect of temperature on modified actin filament length .....	85
4.2.5	Effect of blocking actin on motility in <i>IVMA</i> .....	88
4.3	MODIFIED <i>IVMA</i> QDOT ASSAY RESULT .....	89
4.3.1	Study of Quantum dots optical properties in flow cell .....	89
4.3.2	Modified <i>IVMA</i> with nanoscale cargo attached along actin filament .....	90
4.3.3	Motility analysis with and without QD attachment .....	92
4.3.4	Localization accuracy of immobilized quantum dot .....	93
4.3.5	Linear segment analysis of moving tracks .....	94
4.3.6	Effect of varying ATP concentration on QD sliding velocity .....	96
4.3.7	Estimation of myosin ii motor step size .....	97

Chapter 5: Summary and Conclusions.....	100
Summary .....	101
Conclusions.....	103
Future Work .....	107
References.....	108
List of Publications .....	121
Appendix.....	123
Biodata .....	133

## LIST OF FIGURES

Figure No.	Title	Page No.
1.1	Schematic of typical modified <i>in vitro</i> motility assay with nanoscale cargo attachment and visualization using structured illumination microscopy setup, a super-resolution technique.	6
2.1	The extent of structural organization in chicken skeletal muscle tissue.	11
2.2	The solitary muscle fibre with projecting myofibrils.	13
2.3	Schematic view of sarcomere with the major components. The sarcomere consists of a parallel overlapping array of actin and myosin filaments marked between the Z disc. M region is a bare zone devoid of myosin and contains M protein that connects the myosin filament at the center of the sarcomere.	15
2.4	Schematic representation of conventional myosin ii protein and its corresponding soluble sub-fragments heavy meromyosin and sub-fragments	16
2.5	Schematic illustration of the actin thin filament structure and its regulatory components troponin and tropomyosin.	18
2.6	Monomeric and filamentous form of actin and F-actin depiction using fiber diffraction techniques	20
2.7	The Contraction Mechanism of a Muscle Fibre due to the formation of a cross-bridge between actin and the myosin heads to undergo shortening in the presence of Ca <sup>++</sup> ions within the sarcoplasm	22
2.8	Illustration depicting myosin ATPase cycle chemo-mechanical cycle	24

2.9	Kinetic illustration of actomyosin ATPase reaction. The kinetic cycle shows three phases: detached state 1, weakly bound state 2 (or A.M.D.Pi), and strongly bound post-power stroke state 3 (or A.M.D).	26
2.10	Schematic illustration of one ATP hydrolysis cycle, which represents each myosin head that spends time $\tau_{\text{on}}$ attached to actin and time $\tau_{\text{off}}$ detached from actin	27
2.11	Schematic illustration of the non-processive and processive construct of myosin ii depicting movement on the actin filament	28
2.12	The attachment of various molecular cargo schematically using different types of phalloidin, such as rhodamine phalloidin (RhPh; red), Alexa 488 phalloidin (APh; green), biotin phalloidin (yellow), and phalloidin with variable functionality	29
2.13	Schematic representation of reaction of polystyrene beads with drug and attachment of actin filaments	31
2.14	Illustration of Jablonski profile to show a change in the fluorescent probe's electronic state when photons are excited and emitted.	33
2.15	Diagram illustrating the operational concept of fluorescence microscopy. Specifically, the illustration displays a configuration where a mercury-vapor lamp is used as the source of light. The filter cube in commercial fluorescence microscopes typically combines a dichroic mirror, excitation filter, and emission filter.	34
2.16	Common reporters used in single particle study. The commonly used labeling modules shown include organic dyes, fluorescent proteins, quantum dots (QDs), and gold colloid particles with their corresponding sizes.	37
2.17	The sequence of fluorescent bead images demonstrates the enhancement in image resolution as the number of photons $N$ in the focal point increases.	39

2.18	Illustration of particle localization, connecting the localized spot and image reconstruction	40
2.19	Movements of myosin heads after a load step. a–d, The arrangement of myosin heads, actin filaments, and muscle sarcomeres. e, the length change in nanometers per half-sarcomere (hs) and the load normalized by the isometric force $T_0$ . f, the distribution of axial X-ray intensities relative to the time of X-ray exposure.	41
2.20	Snapshot of two plastic beads held in optical tweezers. A strand of actin that has been fluorescently labeled is stretched out between the beads to perform the mechanical experiment. The bottom part shows the time-dependent displacements of the actin filament along its axis. The movement of a single plastic bead over time was tracked to get the displacement.	42
2.21	The diagram illustrates the stepwise motion of the myosin head immobilized on the scanning probe tips affixed to the glass microneedle to constrain the movement of the myosin head.	44
2.22	Sequential atomic force microscopy (AFM) images depicting the sizes of power strokes (head displacements) that were fitted with a Gaussian distribution. The first power strokes show a mean size of $3.9 \pm 1.1$ nm and the second post-power stroke state with a mean size of $7.9 \pm 2.6$ nm.	45
2.23	The optical tweezer assay conducted on a synthetic myosin rod co-filament to interact with an actin filament. A streptavidin-coated bead is affixed to a biotinylated actin filament and suspended above a myosin-rod co filament.	46
2.24	Representation of MYH7 step size in the time $\times$ space array. The diagram illustrates three distinct time intervals, $\Delta t$ , during which frame capture occurs at $t = t_1, t_2$ , and $t_3$ . During the frame capture of $t_1$ , 5nm step size is measured. During the second interval, $t_2$ ADP is released, producing a step size of 3nm. The third exposure interval exhibits a displacement of 8 nm, resulting from a little step originating from a single actomyosin cycle.	47

2.25	(a) A common design for a molecular shuttle dependent on adsorbed kinesin motors on the surface for transporting a variety of cargo through functionalized microtubules. (b) A typical molecular shuttle in which analytes are collected, labeled, and transported to a detection location.	48
3.1	Sequential steps of myosin ii protein purification from chicken pectoral muscle and protein extraction based on the principle of differential solubility in various buffers followed by protein purification by dialysis.	51
3.2	Design of the flow chamber having nitrocellulose coverslip supported by two strips of double sticky tape. ( <i>J. Sellers 2014, Frontiers in Physiology</i> )	53
3.2	The image on the left panel shows TRITC phalloidin-labeled actin filaments. The image on the right panel shows the obtained tiff image after thresholding by subtracting background noise.	56
3.3	Filament tracking analysis using image J Mtrack 2 plugin. The image on the left panel is labeled filaments or the indexed filaments, and the image on the right panel is the trajectory of corresponding moving actin filaments in the movie, which is used to estimate velocity.	56
3.4	A snapshot of LabVIEW version 10.01.1 was used to calculate filament velocity per frame. The first window showed a motile actin filament opened by the assigned ID for velocity calculation. The second window showed a frame-to-frame velocity plot against the selected frame number. The third window showed the amplitude plot, the average velocity of the specified frame, and the standard deviation values.	57
3.5	The reaction of Sulfo-NHS-LC-Biotin with a primary amine. The yellow oval structure represents the protein with numerous amino groups forming an amide bond with the biotin molecule and sulfo-NHS as the leaving group.	58
3.6	Covalent labeling of polymeric filamentous actin by ester-activated biotin	58
3.7	HABA assay used for biotin quantification by displacement of HABA with biotin-labeled protein from the HABA avidin complex	59

3.8	Schematic representation of non-functional myosin head removal in the <i>in vitro</i> motility assay by blocking actin approach to get functional myosin head in the assay.	61
3.9	Schematic illustration of the single molecule QD <i>in vitro</i> motility assay. A streptavidin conjugated QD walk along biotinylated actin filaments on the nitrocellulose-coated coverslip surface through a layer of immobilized myosin II molecules.	62
3.10	Schematic illustration of sub-pixel localization of super-resolved quantum dots with high accuracy and precision using a MATLAB implementation of the Trackpy Particle-Tracking Toolkit and radial symmetry algorithm	65
3.11	Screening of raw coordinates for considering linear segment analysis.	66
4.1	15% SDS gel pic. Lane 1 corresponds to the ladder, Lanes 2 and 3 correspond to G-actin having a molecular weight of 42 kDa, Lanes 4, 5, and 6 correspond to myosin heavy chain (200 kDa) and its corresponding light chain of 25, 18, and 16 kDa respectively.	68
4.2	Bradford standard curve (myosin ii protein concentration found to be 1.525 mg/ml while actin protein concentration found to be 1.0754 mg/ml).	69
4.3	Snapshot of observed TRITC labeled actin filament sliding velocities ( $\mu\text{m/s}$ ) under fluorescence microscope at controlled conditions. The bound myosin interacts with the actin filament and translocates using energy from ATP hydrolysis.	69
4.4	Sequential snapshots of actin breakage event imaged at 20 frames per second rate.	70
4.5	Sequential snapshots of actin filament rotation event imaged at 20 frames per second rate	71
4.6	Histogram of observed actin sliding velocities ( $\mu\text{m/s}$ ) under controlled conditions of 2mM ATP at 25°C over myosin concentration (100 - 400 $\mu\text{g/ml}$ ). Solid lines are the least	72

	square fit, using a Gaussian equation. The frame-to-frame velocity of ~100 filaments was calculated.	
4.7	Histogram of observed actin sliding velocities ( $\mu\text{m/s}$ ) under controlled conditions of 2mM ATP at 30°C over myosin concentration (100-400 $\mu\text{g/ml}$ ). Solid lines are the least square fit, using a Gaussian equation. The frame-to-frame velocity of ~100 filaments was calculated.	72
4.8	Graph showing the effect of temperature on ensemble average sliding velocity of filament vs myosin surface densities. The average motility increases both with an increase in surface density and temperature. Each data point corresponds to a minimum of 100 sliding filaments' velocity. The points are shown as mean $\pm$ standard deviation.	73
4.9	Histogram of observed actin filament length ( $\mu\text{m}$ ) under controlled conditions, i.e., 2mM ATP at 25°C over myosin concentration (100-400 $\mu\text{g/ml}$ ). Solid lines are the least square fit, using a Gaussian equation. The frame-to-frame velocity of ~100 filaments was calculated. Filament length is found to decrease with an increase in myosin density.	74
4.10	Histogram of observed actin filament length ( $\mu\text{m}$ ) under controlled conditions, i.e., 2mM ATP at 30°C over myosin concentration (100-400 $\mu\text{g/ml}$ ). Solid lines are the least square fit, using a Gaussian equation. The frame-to-frame velocity of ~100 filaments was calculated. Filament length is found to decrease with an increase in myosin density.	75
4.11	Graph showing the effect of temperature on the average length of filament vs myosin surface densities. The average length decreases with an increase in myosin surface density and no change in length with temperature. Each data point corresponds to a minimum of 100 sliding filaments' velocity. The points are shown as mean $\pm$ standard deviation.	76
4.12	<b>A. Top:</b> 8% SDS gel showing the band with varying intensity depending on the amount loaded in the well. <b>Bottom:</b> Relationship between the band intensity (au) and a known amount of myosin. <b>B, Top:</b> 8% SDS gel with eluate from incubated myosin concentrations. <b>Bottom:</b>	77

	Relationship between applied Myosin concentration ( $\mu\text{g/ml}$ ) and myosin molecules/ $\mu\text{m}^2$ .	
4.13	Histogram of observed sliding velocities ( $\mu\text{m/s}$ ) (a) at 2 mM (b) 0.5 mM (c) 0.25mM (d) 0.1 mM ATP (e) 0.05mM (f) 0.025 mM ATP at 30°C over myosin concentration 200 $\mu\text{g/ml}$ . Solid lines are the least square fit, using a Gaussian equation. The points are shown as mean $\pm$ standard deviation.	78
4.14	Histogram of observed sliding velocities ( $\mu\text{m/s}$ ) at 0.001mM ATP (b) Velocity of actin filament as a function of ATP at 200 $\mu\text{g/ml}$ myosin surface density 30°C. The solid line represents Michaelis-Menten fit to filament velocity for a range of [MgATP]. $V_{max}$ and $K_m$ correspond to $5.5\pm 0.8$ $\mu\text{m/s}$ and $0.12\pm 0.06$ .	79
4.15	Snapshot of IVMA images to study the effect of ATP concentration on actin filament length change (a) at 2mM ATP (b) at 0.001mM ATP at 200 $\mu\text{g/ml}$ of myosin surface density and 30°C. The average length of filament at 2mM ATP was $2.76 \pm 0.409$ $\mu\text{m}$ , which was reduced to $0.41 \pm 0.06$ $\mu\text{m}$ at 0.001 mM ATP concentration. The scale bar corresponds to 5 $\mu\text{m}$ .	80
4.16	Histogram of observed actin filament length ( $\mu\text{m}$ ) under varying ATP concentration (a) 2 mM (b) 0.5 mM (c) 0.25mM (d) 0.1 mM ATP (e) 0.05mM (f) 0.025 mM ATP at 30°C over myosin concentration of 200 $\mu\text{g/ml}$ . Solid lines are the least square fit, using a Gaussian equation. The points are shown as mean $\pm$ standard deviation.	80
4.17	Histogram of observed actin filament length ( $\mu\text{m}$ ) at 0.001mM ATP (b) Plot of filament length change as a function of varying ATP concentration at 200 $\mu\text{g/ml}$ myosin surface density 30°C. The points are shown as mean $\pm$ standard deviation.	81
4.18	15% SDS gel pic (A) Lane 1 corresponds to the ladder, and Lane 2 and 3 correspond to actin and biotinylated actin, having a molecular weight of 42 KDa and 43 KDa, respectively. (B) BCA standard curve to calculate the biotin-conjugated actin concentrations.	82

4.19	(A) Micro test plate showing blank, HABA/avidin and HABA/avidin/biotinylated sample at 500nm. (B) IVMA image of Alexa 488 labeled biotinylated actin that interacts with surface-bound myosin ii protein and translocates well in the assay.	83
4.20	Histogram of observed biotin-conjugated actin sliding velocities ( $\mu\text{m/s}$ ) under controlled conditions, i.e., 2mM ATP at 30°C over myosin concentration (a) 100 $\mu\text{g/ml}$ (b) 200 $\mu\text{g/ml}$ (c) 300 $\mu\text{g/ml}$ and (d) 400 $\mu\text{g/ml}$ . Solid lines are the least square fit, using a Gaussian equation. The frame-to-frame velocity of $\sim 100$ filaments was calculated.	84
4.21	Graph showing the effect of biotin conjugation on ensemble average sliding velocity of filament vs myosin surface densities at 30°C, 2mM ATP. The average motility nearly remains the same on biotin labeling. Each data point corresponds to a minimum of 100 sliding filaments' velocity. The points are shown as mean $\pm$ standard deviation.	85
4.22	Histogram of observed biotin-conjugated actin filament length ( $\mu\text{m}$ ) under controlled conditions, i.e., 2mM ATP at 30°C over myosin concentration (100-400 $\mu\text{g/ml}$ ). Solid lines are the least square fit, using a Gaussian equation. The frame-to-frame velocity of $\sim 100$ filaments was calculated. Filament length is found to decrease with an increase in myosin density.	86
4.23	Graph showing the effect of biotin conjugation on filament length vs myosin surface densities at 30°C, 2mM ATP. The average filament length remains the same and decreases with myosin density. Each data point corresponds to a minimum of 100 sliding filaments' velocity. The points are shown as mean $\pm$ standard deviation.	87
4.24	Effect of blocking actin approach on fraction of motile filaments (%) in IVMA on nitrocellulose surfaces studied in the absence and presence of 1 $\mu\text{M}$ blocking actin. Each data point corresponds to 60 filaments from two different myosin preparations.	88

4.25	Actin sliding speed on nitrocellulose surface before ( $5.6045 \pm 0.7987 \mu\text{m/s}$ ) and after ( $5.3955 \pm 0.8097 \mu\text{m/s}$ ) myosin dead head removal treatment at $200 \mu\text{g/ml}$ concentration and $30^\circ\text{C}$ temperature. Bars indicate a mean standard deviation, including at least 60 filaments.	89
4.26	(a) Immobilized quantum dots in a flow cell (b) Variation in light intensity of a single QD observed in a flow cell (c) Intensity plot of QD, FWHM corresponds to 5.2 pixels.	90
4.27	Fluorescence image of quantum dots sliding motility driven by myosin-propelled actin filaments. The IVMA snapshot shows images of moving QDs (red) attached along fluorescent actin filaments (green) labeled with Alexa-488 dye driven by bound myosin ii to nitrocellulose-coated coverslip surface. The scale bar corresponds to $1\mu\text{m}$ .	91
4.28	Fluorescence time series image acquired at 10ms intervals showing single and multiple quantum dots labeled actin filament. The white arrow shows the single labeled quantum dot, and the yellow arrow shows heavily quantum dot labeled filaments. Scale bars correspond to $1\mu\text{m}$ .	92
4.29	Sliding speed of actin filament bound to myosin motor on the nitrocellulose surface before ( $5.207 \pm 0.12 \mu\text{m/s}$ ) quantum dot conjugation and after ( $5.11 \pm 0.63 \mu\text{m/s}$ ) quantum dot conjugation at $200 \mu\text{g/ml}$ myosin concentration and $30^\circ\text{C}$ temperature. Bars indicate a mean standard deviation, including at least 40 entities.	93
4.30	(a) Positional track of immobilized quantum in the <i>in vitro</i> motility assay (b) Histogram of stationary quantum dot fitted by two-dimensional Gaussian function for each image frame (100 fps). Tracking gave a variation in the position of less than 2 nm, suggesting that tracking was possible with $<2$ nm accuracy.	94
4.31	Particle trajectory of moving quantum dots at $0.001 \text{ mM}$ ATP followed by coordinate screening and selection of linear segment for linear path analysis.	95
4.32	Scatter plot of pooled data to analyse relation between simultaneous step of particle in the linear trajectory.	95

	Clustering algorithm was used to find the peaks and Gaussian mixture model was used to obtain multiple mean values. <b>(a)</b> is the step size relation between the d1 and d2 <b>(b)</b> is the step size relation between d1 and d3 <b>(c)</b> is the step size relation between d1 and d4 respectively.	
4.33	Histogram of displacement observed per frame at lower ATP concentration. (a) 0.001 mM ATP (b) 0.025 mM ATP (c) 0.05 mM ATP.	96
4.34	Histogram of displacement observed per frame at higher ATP concentration. (a) 0.1 mM ATP (b) 0.25 mM ATP (c) 0.5 mM ATP (d) 2 mM ATP	96
4.35	(a) Average displacements observed per frame (nm) vs ATP concentration (b) The velocity of the quantum dot as a function of ATP at 200 $\mu\text{g/ml}$ myosin surface density 30°C. The solid line represents the Michaelis-Menten fit. $V_{max}$ and $K_m$ correspond to $5.4 \pm 0.67 \mu\text{m/s}$ and $0.14 \pm 0.05 \text{ mM}$ respectively.	98
4.36	The deconvolution plot for obtained step size per frame (nm) of moving quantum dots at varying ATP concentration with myosin surface density of 200 $\mu\text{g/ml}$ and 30°C temperature. The plot is fitted using multiple peak fit function in the origin and the solid line represents Gaussian fit analysis.	98

## LIST OF TABLES

<b>Table No.</b>	<b>Title</b>	<b>Page No.</b>
2.1	The covalent conjugation approach for actin filament using various functional groups and cross-linkers	30
2.2	Characteristic features of fluorescent proteins (FPs), organic dyes (ODs), and quantum dots (QDs) as probes for use with single-molecule applications.	38
2.3	Effect of quantum dot attachment on myosin-induced actin sliding at a varying ATP concentration	99

## ABBREVIATIONS AND SYMBOLS

ADP	Adenosine Diphosphate
ATP	Adenosine Triphosphate
$\beta$ ME	2- $\beta$ Mercapto Ethanol
BSA	Bovine serum albumin
EMCCD	Electron Multiplying Charge Coupled Device
ELC	Essential Light Chain
$\text{Ca}^{2+}$	Calcium (divalent ions)
CrP	Creatine Phosphate
CPK	Creatine Phosphokinase
$d$	Working stroke of myosin II motor
DTT	Dithiothreitol
EDTA	Ethylene Diamine Tetraacetic Acid
EGTA	Ethylene Glycol Tetraacetic Acid
HMM	Heavy Meromyosin
IVMA	<i>In Vitro</i> Motility Assay
KCl	Potassium chloride
$k_{ADP}$	Rate constant for ADP release
$k_{ATP}$	Second-order rate constant of ATP binding

kDa	Kilo Dalton
$K_m$	Apparent binding constant for [MgATP]
$k_{-Pi}$	The rate constant for the Pi release
KPi	Potassium phosphate buffer
LMM	Light Meromyosin
MgCl <sub>2</sub>	Magnesium chloride
mM	Millimolar
MOPS	3 - (N-morpholino) propane sulfonic acid
NaN <sub>3</sub>	Sodium Azide
PMSF	Phenylmethylsulfonyl fluoride
Pi	Inorganic Phosphate
RLC	Regulatory Light Chain
S1	Sub-fragment 1
S2	Sub-fragment 2
sCMOS	Scientific Complementary Metal Oxide Semiconductor
S.D	Standard Deviation
S.E	Standard Error
SDS PAGE	Sodium Dodecyl Sulfate Poly Acrylamide Gel Electrophoresis
Tm	Tropomyosin
Tn C	Troponin C
Tn I	Troponin I
Tn T	Troponin T

$T_{on}$	Time of attachment
Tris-Cl	Tris hydrochloride
TRITC	Tetramethyl Rhodamine Isothiocyanate
$V_F$	Velocity of thin filament sliding in the <i>IVMA</i>
$V_{max}$	Velocity of thin filament sliding at saturating [MgATP]
NA	Numerical Aperture
SNR	Signal-to-noise Ratio
SRM	Super-resolution microscopy
SIM	Structured Illumination microscopy
QD	Quantum dot
HABA	4'-hydroxy azobenzene-2-carboxylic acid
mL	Millilitre
PBS	Phosphate buffer saline
$\mu\text{g}$	Microgram
$\mu\text{L}$	Microlitre
AFM	Atomic force microscopy
RT	Room Temperature
mg	Milligram
EDC	N-(3-Dimethylaminopropyl)-N'-ethyl carbodiimide hydrochloride)
NHS	N-Hydroxy succinimide
$^{\circ}\text{C}$	Degree Celsius

min	Minute
ml	Millilitre
mM	Millimolar
ng	Nanogram
nM	Nanomolar